A Pyk2 Inhibitor Incorporated into a PEGDA-Gelatin Hydrogel Promotes Osteoblast Activity and Mineral Deposition

Sumana Posritong[1], Regina Flores Chavez[1], Tien-Min G. Chu[1], and Angela Bruzzaniti[1]*
Department of Biomedical and Applied Sciences, Indiana University School of Dentistry, Indianapolis, Indiana, 46202, USA

*Corresponding author: Dr. Angela Bruzzaniti
Department of Biomedical and Applied Sciences, Indiana University School of Dentistry, 1121 W. Michigan Street, DS243, Indianapolis, IN 46202.
E-mail: abruzzan@iu.edu

Abstract

Pyk2 is a non-receptor tyrosine kinase that belongs to the family of focal adhesion kinases. Studies from our laboratory and others demonstrated that mice lacking the Pyk2 gene (*Ptk2B*) have high bone mass, which was due to increased osteoblast activity, as well as decreased osteoclast activity. It was previously reported that a chemical inhibitor that targets both Pyk2 and its homolog FAK, led to increased bone formation in ovariectomized rats. In the current study, we developed a hydrogel containing poly(ethylene glycol) diacrylate (PEGDA) and gelatin which was curable by visible-light curable and was suitable for the delivery of small molecules, including a Pyk2-targeted chemical inhibitor. We characterized several critical properties of the hydrogel, including viscosity, gelation time, swelling, degradation, and drug release behavior. We found that a hydrogel composed of PEGDA1000 plus 10% gelatin (P1000:G10) exhibited Bingham fluid behavior that can resist free flowing before *in situ* polymerization, making it suitable for use as an injectable carrier in open wound applications. The P1000:G10 hydrogel was cytocompatible and displayed a more delayed drug release behavior than other hydrogels we tested. Importantly, the Pyk2-inhibitor-hydrogel retained its inhibitory activity against the Pyk2 tyrosine kinase, and promoted osteoblast activity and mineral deposition *in vitro*. Overall, our findings suggest that a Pyk2-inhibitor based hydrogel may be suitable for the treatment of craniofacial and appendicular skeletal defects and for targeted bone regeneration.

Keywords: osteoblast, bone formation, alkaline phosphatase, tyrosine kinase, mineralization

---

This is the author's manuscript of the article published in final edited form as:

Posritong, S., Chavez, R. F., Chu, T.-M. G., & Bruzzaniti, A. (2019). A Pyk2 inhibitor incorporated into a PEGDA-gelatin hydrogel promotes osteoblast activity and mineral deposition. Biomedical Materials, 14(2), 025015. https://doi.org/10.1088/1748-605X/aafffa

1. Introduction

The repair of bone damage including large bony defects resulting from trauma, infection, tumor, and skeletal abnormalities is challenging due to their large size and the need to maintain stability and cytocompatibility. The current gold standard treatment for the regeneration of bony defects is the use of autologous grafts because they possess inherent osteoconductivity, osteoinductivity, and osteogenicity. However, there are a limited number of skeletal sites from which large grafts can be harvested and concerns for donor site morbidity remain [1, 2]. Bone tissue engineering techniques that use biomolecules or drugs incorporated into scaffolds have been investigated as an alternative approach for bone grafting [3, 4]. Among these biomolecules, BMP-2 is a well-documented growth factor for bone regeneration in orthopedic and maxillofacial applications [3, 5-7], although clinical concerns exist such as increased risk of radicular pain, ectopic bone formation and osteolysis. These limitations suggest a continued need for that alternative biomolecules for bone regeneration and bone tissue engineering remains [8-11].

The proline-rich tyrosine kinase, Pyk2, belongs to the family of focal adhesion kinases, and regulates the proliferation, adhesion and migration of mesenchymal cells [12-18]. We and others have shown that Pyk2 genetic deletion leads to increased bone bass, through both increased bone formation by osteoblasts and decreased bone-degradation by osteoclasts [16, 19]. Further, we reported that Pyk2-deficient osteoblasts show increased proliferation and mineral deposition than wild-type (WT) osteoblasts, and that the osteogenic effect of Pyk2-deletion was associated with the estrogen signaling cascade [20]. Further, it was shown that ovariectomized rats treated with the chemical inhibitor PF-431396 (PF-43), which targets both Pyk2 and the related protein FAK, had increased bone formation and were protected from ovariectomy-induced bone loss [16]. A new Pyk2-targeted inhibitor PF-4618433 (PF-46) was subsequently developed and shown to enhance alkaline phosphatase (ALP) activity and mineral deposition by human mesenchymal stem cells (MSCs) *in vitro* [21]. These findings suggest that a Pyk2-inhibitor based scaffold may be useful for targeted osteogenic applications.

Drug delivery systems such collagen sponges have been proven for safety and efficiency for bone regeneration [22]. However, collagen sponges exhibit an initial uncontrolled burst release that can damage surrounding tissues. A better alternative for controlled drug delivery is poly(ethylene glycol) (PEG) [23, 24]. PEG-diacrylate (PEGDA), a PEG-based macromer with reactive termini, has extensively been used in hydrogel fabrication because of the simplicity of its synthesis and its commercial availability [25]. However, the PEGDA solution is a low viscosity fluid that is difficult to use for *in situ* polymerization applications, such as the repair of segmental long bone defects. It is known that the incorporation of gelatin into matrices enhances their biological characteristics because gelatin contains cell-recognition motifs such as RGD sequences, and gelatin can be cleaved by various proteases such as matrix metalloproteinase MMP-2 and MMP-9, which can improve the biodegradability of the system. [26, 27]. Furthermore, a semi-

interpenetrating network (sIPN), which contains photocrosslinked PEG matrices and physically entrapped gelatin, has been developed as an effective drug delivery and tissue engineering scaffold [28]. sIPN of PEG matrices improves protein resistance and mechanical stability. Therefore, we postulated that incorporation of gelatin into a PEGDA prepolymer solution would enhance the viscosity of solution, and consequently improve the handling of prepolymer solution.

In the current study, we developed a new PEGDA-gelatin hydrogel which was suitable as a carrier scaffold for small molecules, including the Pyk2-inhibitor, PF-461-8433 (PF-46). We found that the PEGDA-gelatin hydrogel is an effective carrier in terms of its viscosity and material handling properties, hydrogel biodegradability and drug release behavior. The Pyk2-inhibitor releases from the PEGDA-gelatin hydrogel retained its bioactivity and was effective in promoting osteoblastic bone formation *in vitro*. These findings suggest that PEGDA-gelatin hydrogels are suitable for the delivery of small molecules such as the Pyk2 inhibitor, and therefore will have broad applications for targeted bone regeneration.

2. Materials and Methods

2.1. Materials

Hyclone α-MEM, L-glutamine and penicillin/streptomycin (P/S) were purchased from Thermo Fisher, NY, USA. Fetal Bovine Serum (FBS) was from Biowest, MO, USA. PF-431396 (PF-43) [16] was purchased from Sigma, MO, while PF-4618433 (PF-46) [21] was purchased from Adipogen CA (USA). Resorbable RCF collagen sponges were purchased from the Surgical Supplies Co. Brockton, MA, USA. Type B gelatin from bovine skin and 7-amino-4-methylcoumarin were from Sigma-Aldrich. PEGDA 1000 Da and 600 Da was purchased from Polysciences Inc, Warrington, PA (USA). The LAP photoinitiator and dithiothreitol were from Sigma. The CellTiter 96® AQeous Non-Radioactive Cell Proliferation Assay kit was from Promega, WI, USA. Ascorbic acid, β-glycerol phosphate and p-nitrophenyl phosphate in 1.5 M alkaline buffer, Alizarin Red S, cetyl pyridinium chloride and Type B gelatin were all purchased from Sigma.

2.2. Cell culture

Murine bone marrow-derived mesenchymal stem cells were used our source of stromal pre-osteoblast/osteoblast cells (BMSCs) and were obtained from tibia and femur of 8-14 week-old C57BL/6 mice. Both proximal and distal ends of the tibia and femur were cut away from the epiphysis, and the marrow was flushed out with PBS. The released cells were collected and cultured in α-MEM with L-glutamine (Hyclone, UT, USA) supplemented with 10% (v/v) FBS and 1% (v/v) penicillin/streptomycin (P/S, Lonza, NJ, USA) in an incubator at 37ºC with 5% CO_2. The medium was changed after 24 hours and non-adherent cells were removed. Cells were cultured until confluent and then trypsinized and plated in new dishes. All experiments used BMSCs from the second passage. All mice used in this study were

handled according to the guidelines of the American Association for Laboratory Animal Science using Institutional Animal Care and Use Committee (IACUC) approved protocols and in according with the NIH (Guide for the Care and Use of Laboratory Animals, 1996).

MC3T3-E1 mouse osteoblastic cell line were originally purchased from the American Type Culture Collection (ATCC). 293VnR cells were developed as previously reported [29]. Aliquots of cells were stored frozen in liquid nitrogen. Frozen cells were thawed and grown in α-MEM with L-glutamine supplemented with 10% (v/v) FBS and 1% (v/v) P/S in an incubator at 37ºC with 5% CO_2.

2.3. Cell proliferation assay

To examine the effect of PF-431396 (PF-43) and PF-4618433 (PF-46) on the proliferation of osteoblasts, BMSC were plated at 2×10^3 cells/well of 96-well plate in the presence or absence of 0 - 0.3 μM of each inhibitor for 24 hours. A MTS assay using the CellTiter 96® AQeous Non-Radioactive Cell Proliferation Assay kit was then performed. The absorbance at 490 nm was measured using a spectrophotometer. Experiments were performed in triplicate and repeated three times independently.

2.4. Alkaline phosphatase (ALP) activity assay

BMSC were plated at 4×10^4 cells and differentiated into mature osteoblasts with 50 μM ascorbic acid (AA) and 5 mM β-glycerol phosphate (β-GP) in the presence or absence of various concentration of PF-43 or PF-46 for 7 days. ALP activity assay was assayed by adding cell lysate to the ALP substrate containing 2 mg/mL p-nitrophenyl phosphate in 1.5 M alkaline buffer as previously reported [17, 18]. The enzymatic reaction was stopped by adding 20 mM NaOH, and optical absorbance at 405 nm was recorded using a spectrophotometer. ALP activity was normalized by total protein concentration using a Pierce™ BCA protein assay kit. Experiments was performed in triplicate and repeated three times.

2.5. Quantification Alizarin Red S staining

BMSC were plated at 4×10^4 cells/well in the presence or absence of various concentration of PF-43 or PF-46 and differentiated into mature osteoblasts under osteogenic conditions containing for up to 21 days. Osteoblasts were fixed and stained with 40 mM Alizarin Red S (pH 4.2), which stains bound calcium-stained mineral deposits, as previously reported [17, 18, 30]. Alizarin-stained cells were imaged. Alternatively, the wells were washed extensively after staining, the bound Alizarin Red S was extracted with 1% cetyl pyridinium chloride in 10 mM sodium phosphate (pH 7.0) and the absorbance was measured at 562 nm. Ca2+ deposition was quantified against an Alizarin Red S standard curve. Experiments were performed in triplicate and reproduced 3 times.

2.6. Hydrogels preparation

PEGDA 600 Da or 1000 Da was dissolved in α-MEM at 37°C under stirring to form a 50% w/v (0.5 g/mL) solution overnight. To this, 2% (0.02 g) lithium phenyl-2,4,6-trimethylbenzoylphosphinate (LAP) photoinitiator, and 0.1 mM dithiothreitol (DTT) were added and stirred for 8 hours [31, 32]. Type B gelatin was also dissolved in α-MEM at 37 °C under stirring to form 10% w/v (0.1 g/mL) or 20% (0.2 g/mL) solution overnight, and the pH adjusted to 7.2. Next, PEGDA solution was mixed with gelatin solution at ratio 1:1 by volume under stirring to obtain the following gel formulations: 1) PEGDA1000 plus 10 % gelatin (P1000:G10). 1 mL of PEGDA1000 was combined with 1 mL of the 20% gelatin solution to form a hydrogel with the final concentration of 25% PEGDA1000 plus 10% gelatin, or 2.5 g PEGDA1000 plus 0.1 g gelatin. 2) PEDGA600 plus 5% gelatin (P600:G5). 1 mL of PEGDA600 was combined with 1 mL of the 10% gelatin solution to form a hydrogel with the final concentration of 25% PEGDA600 plus 5% gelatin, or 2.5 g PEGDA600 plus 0.05 g gelatin. 3) 25% PEGDA1000 (P1000). 4) 25% PEGDA600 (P600). All the concentrations indicated were the final concentration in the prepolymer solution. Aliquots of the prepolymer solution (150 μL each) were pipetted into disk-shaped silicone molds of 5 mm in diameter and 3 mm in thickness, and then exposed under LED light 450-470 nm and 1000 J/cm2 for 2-6 minutes to achieve complete photopolymerization. A schematic representation of the preparation of hydrogels, and the subsequent characterization analyses and osteoblast osteogenic studies with eluted PF-46 are shown in Figure 2.

2.7. Dynamic viscosity test

Dynamic viscosity of the prepolymer solutions (1 mL) was measured on a Bohlin CVO 100 digital rheometer (viscometry mode) using 4° cone/plate geometry in controlled shear rate at 100 to 600 s^{-1} with a gap size of 150 μm at room temperature [33].

2.8. Determination gelation time

Gelation times of the P600, P600:G5, P1000, and P1000:G10 prepolymer solutions were determined using a technique as described previously [34, 35]. Briefly, the prepolymer solution 150 μL was pipetted into the disk-shaped silicone mold of 5 mm in diameter and 3 mm in thickness and exposed under visible LED light 450-470 nm and 1000 J/cm^2 for 20 seconds; then a periodontal probe was used to contact the surface. This contact was repeated at 20-second intervals throughout the duration of light exposure. Gelation time was defined as the time when the surface of materials hardened and materials did not adhere to the tip of the periodontal probe. This experiment was carried out at the room temperature (N=5/group).

2.9. Swelling and degradation

The swelling and degradation of our hydrogels was determined as reported previously [31, 32]. Hydrogels were prepared (N=5/group) as described above and were dried under the vacuum for 48 hours to completely remove remaining water. The initial dry weight of hydrogel was measured. Hydrogels were immersed in 1 mL of pH 7.4 PBS in microfuge tubes and stored at 37°C. Hydrogels were removed from the tubes every 30 minutes for the first four hours, and then at 24, 48, 72, 120, 240, 360, 480, and 600 hours. Immediately after removal, hydrogels were dried with Whatman paper to remove excess water and then weighed. One mL of fresh PBS was used at every time point to keep the volume constant. The percentage of swelling ratio (*Q*) was then calculated as: $Q = \frac{Wt}{Wd} \times 100\%$. *Wt* is wet weight at time t, and *Wd* is dried weight of hydrogels. To quantify hydrogel degradation, we performed a hydrolytic degradation assay. The extent of degradation (D) was calculated on day 3, 5, 10, 15, and 25 using the following equation: $D = \left[1 - \frac{mt}{mi}\right] \times 100\%$. *Mt* is the gel mass at a particular time point and *mi* is the gel mass at 48 hours.

2.10. FTIR analysis of hydrogels

To characterize the chemical characteristics of the hydrogels, PEGDA600, 10% gelatin stock solution, cured P600:G5, PEGDA1000, 20% gelatin stock solution, and cured P1000:G10 were evaluated by fourier transform infrared spectroscopy (FTIR) as previously reported [36] using the attenuated total reflection mode (FT/IR-4100, JASCO Analytical Instruments, Easton, MD, USA), at a resolution of 4.0 cm^{-1} from 1500 to 2800 cm^{-1}.

2.11. Cytotoxicity of hydrogels

The cytotoxicity of hydrogels against MC3T3-E1 osteoblastic cells was evaluated by following the guidelines of the International Organization for Standardization (ISO 10993-5) [37]. Hydrogels and collagen sponge disks (N = 5/group) were prepared as above. All samples were sterilized by UV light for 30 minutes per side. Each sample was immersed in 1 mL of α-MEM with L-glutamine supplemented with 10% (v/v) FBS and 1% (v/v) P/S in an incubator at 37ºC for 24 hours. Eluates from each group were then collected. MC3T3-E1 were seeded at 1.5×10^3 cells per well in 96-well plate and incubated overnight at 37°C with 5% CO_2. Thereafter, the medium was replaced with 150 µL of eluates from the scaffolds. For the control group, fresh medium was used. After incubation for 24 hours, the CellTiter 96®AQeous Non-Radioactive Cell Proliferation Assay kit was used.

2.12. In vitro drug release behavior

We initially used 7-amino-4-methylcoumarin (AMC), a fluorogenic compound, as a test molecule to determine the drug release behavior of our hydrogels. AMC detection can be readily accomplished using

370 nm excitation and 460 nm emission wavelengths. Therefore, we compared the release behavior of the hydrogels with collagen sponges [38] using AMC as a test drug due to its ease of use. Collagen sponges were cut into disks of 5 mm in diameter and 3 mm in thickness using a hole-puncher and then loaded directly with an equivalent volume of AMC.

Hydrogel disks and collagen sponges were prepared as described above (N=5/group). 50 μg of AMC was added directly to collagen sponge, or added to the prepolymer hydrogel solution before photopolymerization. Samples from each group were soaked in 1 mL of PBS and stored in an incubator at 37ºC for 24 hour. Samples from all groups were then sonicated. To determine the amount of 7 AMC that was successfully loaded into the scaffolds, the total amount of AMC released into the PBS was measured using a Biotek Synergy HTX multi-mode reader at 370 nm excitation and 460 nm emission wavelengths. The loading efficacy was calculated as follows: % loading efficacy = $\frac{amount\ of\ drug\ in\ the\ scaffold}{drug\ added} \times 100$

For the release profile of AMC over time, samples were soaked in 1 mL of PBS at 37°C, and 500 μL of the soaking solution was collected on day 0, 1, 2, 3, 5, 10, 15, 20 and 25, to measure the AMC amount using a Biotek Synergy HTX multi-mode spectrophotometer (n=5/group). The samples were replaced with fresh 500 μL of PBS at every time point in order to keep a constant volume. The concentration of release AMC was calculated from a standard curve of AMC.

The drug release profile of P1000:G10 containing a final concentration of 20 μM PF-46 or equivalent volume of the DMSO vehicle control were evaluated as above. PF-46 was added to the P1000 prior to the addition of gelatin to a final concentration of 20 μM (17.82 μg), after which 150 μl of the hydrogel was immediately loaded into molds, and light cured. The disks were released from the mold, and immersed in 250 μl serum free α-MEM (required for subsequent cell-based studies) for a final volume of 400 μl of P1000:G10 hydrogel containing PF-46. The hydrogel was incubated at 37ºC for 1, 2, 3, 4, 24, 48, 72, 96 hours. At each time point, 50% of the solution was removed and replaced with the same volume of fresh α-MEM. The percentage loading efficacy was calculated using a spectrophotometer based on the reported emission wavelength for PF-46. A standard curve was generated for PF-46 (after subtracting the DMSO baseline) and used to calculate the release profile of PF-46 from the hydrogel. The % cumulative release of PF-46 from the P1000:G10 hydrogel was calculated as described above. Experiments were performed in triplicate and mean ± SEM was determined.

2.13. In vitro kinase activity assay

PF-46 (20 μg) loaded hydrogels were prepared, sterilized by UV, and then soaked in α-MEM with 10% FBS and 1% P/S at 37ºC for 24 hours. The concentration of PF-46 was estimated based on the release behavior calculated for loaded hydrogels after 24 hours. Three days prior to conducting the kinase assay,

293VnR cells were transfected with Pyk2 cDNA. 293VnR cells were used in this assay because they do not express Pyk2 and reveal high efficiency in transfection [29]. Pyk2-expressing 293VnR cells were then treated for 2 hours with released PF-46 at various concentrations (N = 5/group). For the positive and negative controls, Pyk2-expressing 293VnR cells were incubated with fresh PF-46 at 0.1 and 0.3 μM concentrations (positive-controls) or left untreated (negative) control group. In addition, Pyk2-expressing 293VnR cells were immunoprecipitated with an anti-Pyk2 antibody and blotted for Pyk2 (EMD Millipore, MA, USA) to confirm that all groups had the same level of Pyk2. After this, a tyrosine kinase activity assay was performed following the manufacturer's protocol (Takara Bio, CA, USA).

2.14. Statistical analyses

All data were analyzed by one-way analysis of variance (ANOVA) followed by post hoc multiple comparisons where appropriate. Data was analyzed by using SPSS 24 software (IBM Corporation, Armonk, NY, USA). Data is presented as means ± standard error of means (SEM), and a statistically significant difference was determined at $p \leq 0.05$.

3. Results

3.1. The Pyk2 inhibitor, PF-46, enhances osteoblast proliferation, matrix formation and mineralization.

First, we compared the effects of two Pyk2 inhibitors, PF-43 is reported to be a dual Pyk2/FAK inhibitor, and PF-46, which is more highly selective for Pyk2. We examined the effect of PF-43 and PF-46 on the proliferation of osteoblast precursors. PF-43 (0.1 and 0.3 μM) and PF-46 (0.3 μM) significantly increased cell proliferation activity when compared to the untreated or control group ($p<0.05$). Moreover, 0.1 μM PF-46 exhibited the highest proliferation activity among the groups ($p<0.05$) (Figure 1A).

We next examined the effect of the inhibitors on the activity of mature osteoblasts, using the ALP and mineralization assays. ALP is an enzyme expressed in the membrane of active osteoblasts and is essential for the ability of osteoblasts to produce un-mineralized osteoid, which is then later mineralized by the mature osteoblasts [39]. During the differentiation process, pre-osteoblasts mature to osteoblasts and then differentiate further to become mineralizing osteoblasts. This involves the temporal and linear expression of necessary genes/proteins. To induce the differentiation of BMSCs into osteoblasts, BMSCs were cultured with 50 μM ascorbic acid and 5 mM β-GP in the presence or absence of PF-43 or PF-46, or vehicle control (DMSO). Since ALP activity peaks before the peak for maximal mineral deposition, we examined the effect of the inhibitors by quantifying ALP activity at 7 days, and mineral deposition at later time points (14 or 21 days). Our results revealed that both PF-43 and PF-46 at 0.1 and 0.3 μM significantly increased ALP activity (Figure 1B). However, calcium deposition, which is a marker of the mineralizing activity of osteoblasts, was only enhanced by PF-46 at the concentrations examined (0.1 and 0.3 μM), with

PF-43 showing no effect on calcium deposition at these concentrations (Figure 1C). Given that PF-46 increased both ALP and mineral deposition, our findings suggest that PF-46 promotes differentiation from immature to mature mineralizing osteoblasts, whereas PF-43 is only able to promote the early stages of the osteoblast differentiation process during which ALP is active. Based on our finding that PF-46 promotes ALP activity and mineralization to a greater extent than PF-43, the dual Pyk2/FAK inhibitor, we used PF-46 for all subsequent studies.

3.2. P1000:G10 prepolymer solution reveals Bingham fluid behavior with a yield point.

To measure the dynamic viscosity of the prepolymer solutions, all prepolymer solutions were prepared and examined for the controlled shear rate viscometry using a digital rheometer (viscometry mode) at room temperature. Our results demonstrated that all groups exhibited shear-thinning behavior. Furthermore, the addition of gelatin enhanced the shear-thinning effect in both P1000 and P600 prepolymer solutions (Figure 3A). After prepolymer solutions reached Newtonian fluid behavior and exhibited a constant viscosity, P1000:G10 revealed the highest viscosity (44.8 mPa.s), followed by P600:G5 (39.1 mPa.s), P1000 (28.5 mPa.s) and lastly P600 (16.4 mPa.s).

Yield stress is the applied stress that needs to be exceeded in order to make materials flow. A material with this property is called a Bingham fluid or yield stress fluid, which is fully elastic when the stress value is below the yield stress, but it flows at stresses above yield stress [40]. Regarding the plot of shear stress versus the shear rate or the flow curve (Figure 3B), incorporating gelatin into the PEGDA1000 prepolymer solutions allowed P1000:G10 solution to demonstrate a yield stress of about 16 Pa. This property allows the prepolymer solution to remain localized when delivered, and is not free-flowing before the solution is polymerized by light curing.

3.3. *Determination of hydrogel gelation times.*

The gelation times of P600, P600:G5, P1000, and P1000:G10 are shown in Figure 4. The statistical analysis indicated significant differences in the gelation times among the groups ($p<0.05$). The shortest mean gelation time (2.17±0.17 minutes) was recorded for P600. No significant difference in the gelation time was found between P600 and P600:G5. However, both P1000 and P1000:G10 showed a significantly higher gelation time than P600 and P600:G5. P1000:G10 exhibited the significantly longest gelation time when compared to the other groups (5.4±0.15 minutes, $p<0.05$). We can see that both P600:G5 and P1000:G10 exhibited a gelation time between 2-6 minutes, which is acceptable and feasible for *in situ* polymerization. Regarding the viscosity, P600:G5 and P1000:G10 had shear-thinning effect and a high viscosity and yield stress fluid. These finds suggest these hydrogels can be used as injectable carriers and the solutions will not

be free-flowing before *in situ* photopolymerization. Therefore, P600:G5 and P1000:G10 hydrogels were chosen for all subsequent experiments.

3.4. P600:G5 shows a greater swelling behavior and degradation than P1000:G10.

The swelling behavior of hydrogels can greatly affect the pore size of network and drug release behavior of gels. We evaluated the swelling ratio (Q) of PEGDA-gelatin hydrogels by soaking gels in PBS at 37°C and weight measuring up to 25 days. Both P1000:G10 and P600:G5 gels revealed rapid water absorption and swelling and reached a maximum swelling ratio (Q_{max}) within 1 and 1.5 hours, respectively (Figure 5A). P1000:G10 showed significantly lower Q_{max} than P600:G500 ($p<0.05$). There were no difference in the percent weight loss between P600:G5 and P1000:G10 at day 25 (Figure 5B).

3.5. Chemical characterization of uncured and cured hydrogels

To characterize the chemical characteristics of the hydrogels, PEGDA 600 (P600), 10% gelatin stock solution, cured P600:G5, PEGDA 1000 (P1000), 20% gelatin stock solution, and cured P1000:G10 were evaluated by FTIR. As shown in Figure 6, The FTIR spectrums clearly showed the C=C stretch around 1634 cm^{-1} from 50% PEGDA 600 solution and PEGDA 1000 solution in α-MEM. Carboxylic acid C=O stretch around 1705 cm^{-1} from the acids in α-MEM can also be seen. Amide I C=O stretch can be seen in the two gelatin samples around 1630 cm^{-1}. Amide II N-H deformation can also been seen in the 20% gelatin solution around 1550 cm^{-1}.

3.6. P1000:G10 hydrogels exhibit the highest loading efficiency and the slowest release behavior.

The loading efficiency mostly depends on the drug or substance solubility in the scaffold matrix material, the composition and molecular weight of the polymer, and the drug–polymer interaction [41]. Resorbable collagen sponges are widely used as carrier for biomolecules for regenerative applications [38, 42]. Therefore, we compared the drug release behavior of hydrogels with drug-loaded collagen sponges. Similar to other published studies using coumarin-based fluorochromes, we used the fluorogenic compound, AMC, as a model to determine the drug release characteristics of our hydrogels [43]. As a control, collagen sponges, which are commonly used as drug carriers, were also loaded with a similar amount of the AMC compound. We determined the total amount of AMC released from the candidate carriers as shown in Figure 7A. The AMC-loaded collagen sponges showed a loading efficiency of 100%, while the loading efficiencies in P1000:G10 and P600:G5 were 99% and 83%, respectively.

For the release behavior of the PEGDA-gelatin hydrogels compared to the collagen sponge, we also used AMC. The hydrogels and collagen sponges loaded with AMC were soaked for 1-25 days, and aliquots of the fluorochrome were measured at different time intervals. The percentage of cumulative *in*

vitro release patterns of AMC loaded PEGDA-gelatin hydrogels and collagen sponges are shown in Figure 7B. On day 3, the cumulative initial burst of dye released from P1000:G10, P600:G5, and control were approximately 84%, 88%, and 93% of the loading amount, respectively. Approximately 100% of the loaded fluorochrome was released from the control group by day 5, followed by P600:G5 at day 10 and P1000:G10 at day 15.

Biomolecule release from hydrogels generally occurs through the mechanisms of diffusion, erosion, or degradation [23, 26]. We examined the impact of diffusion on drug release mechanism of the hydrogels. A simple mathematical method to determine the release kinetics of molecules from a polymer matrix is derived by plotting the first 60% of cumulative drug release data vs. square root of time (Figure 7B and insert), then fitting data in the Higuchi equation: $Q_t = Kt^{1/2}$, where Q_t is the amount of drug released at time t, and K is the release constant rate. This equation is based on the Fickian diffusion and applicable to the diffusion of drugs that dispersed homogeneously in a polymer matrix [44, 45]. By applying this model to our hydrogels, we found that data from all groups acceptably fit this equation ($R^2 > 0.96$). This finding indicated that the drug release mechanism of P1000:G10, P600:G5, and collagen sponge followed Fickian diffusion with the K values at 46.68±1.28, 48.68±1.27, and 49.59±1.73, respectively.

As the P1000:G10 performed better than P600:G5 on our hydrogel characterization tests, we then confirmed that PF-46 loaded into P1000:G10 hydrogel exhibited a similar release profile to AMC in the hydrogel. We generated P1000:G10 hydrogels containing PF-46, and examined the release profile of PF-46 over 1-4 days (which was based on the peak elution of AMC from P1000:G10). The % cumulative release behavior of PF-46 was determined as described above and described in the methods. As shown in Figure 7C, PF-46 exhibited a % cumulative release profile that showed an initial burst release (1-4 hours) followed by a slower release over the remaining 1-3 days, which was overall similar to the AMC profile. 100% release of PF-46 was achieved by days 3-4 in our culture conditions.

3.7. P1000:G10 and P600:G5 hydrogels are non-cytotoxic carriers

According to the guidelines of the International Organization for Standardization (ISO 10993-5) [37], biomaterials that exhibit ≥70% relative cell viability compared to the control group are considered to be non-cytotoxic materials. Therefore, we examined whether the P600:G5 and P1000:G10 hydrogels exhibited cytotoxic effects on osteoblastic cells. We collected eluates of P1000:G10 and P600:G5 hydrogels and cultured MC3T3-E1 cells (a pre-osteogenic cell line) in these eluates for 24 hours, followed by MTS assay. We found that the cell viability was 70% and 80% for the P1000:G10 and P600:G5 eluates, respectively (Figure 8). Using either media alone or collagen sponge eluates as controls, the MC3T3-E1 cell viability was found to be 100%. These data suggest that both P1000:G10 and P600:G5 hydrogels are likely to be non-cytotoxic to osteogenic cells, with cell viability ≥70% after 24 hours.

Therefore, for subsequent experiments, we chose the P1000:G10 hydrogel as the carrier for PF-46 due to its improved viscosity, compared to P600:G5, combined with its acceptable gelation time, release behavior, and cytocompatibility.

3.8. PF-46 released from hydrogels retains its efficacy to inhibit Pyk2 kinase activity

We examined if PF-46 released from P1000:G10 hydrogels retains its ability to inhibit Pyk2 tyrosine kinase activity (Figure 9). We first expressed Pyk2 cDNA in 293VnR fibroblast cells by transient transfection. Expressed Pyk2 was immunoprecipitated a protein-G agarose and anti-Pyk2 antibody. We confirmed by Western blotting that all groups expressed the same level of Pyk2 (Figure 9B). Immunoprecipitated Pyk2 was incubated with PF-46 released from the P1000:G10 hydrogels and then used in a tyrosine kinase activity assay. We found that all concentrations of released PF-46 significantly inhibited Pyk2 tyrosine kinase activity when compared to the no-drug control group ($p<0.05$, Figure 9A). The inhibitory effect of released PF-46 (0.1, 0.3 and 0.5 μM) on Pyk2 kinase activity was comparable to freshly prepared PF-46 that had not previously been loaded in the hydrogel.

3.9. Hydrogel-released PF-46 enhances ALP activity and mineralization of osteoblasts

We examined the osteogenic bioactivity of PF-46 released from the P1000:G10 hydrogels. BMSCs were differentiated into mature osteoblasts under osteogenic conditions in the presence or absence of the released PF-46, using the estimated concentrations of 0.1 and 0.5 μM. Also included were control BMSCs, BMSCs incubated with freshly prepared PF-46, or with PF-46 (no hydrogel) pre-incubated at 37°C for 24 hours prior to use (used as control for the effect of culture time and temperature on the stability of PF-46). ALP activity was quantified after 7 days of culture. As shown in Figure 10A, released PF-46 at 0.1 and 0.5 μM markedly enhanced ALP activity, compared to either the zero control or the non-loaded P1000:G10 group ($p<0.05$). Furthermore, the ALP activity of osteoblasts treated with released PF-46 at 0.1 and 0.5 μM was not statistically different from PF-46 incubated for 24 hours at 37°C. These data suggest that PF-46 released from P1000:G10 hydrogels retains its ability to promote osteoblast activity.

We examined whether hydrogel-released PF-46 also improved Ca^{2+} mineral deposition by BMSCs, which is marker of mature osteoblasts capable of bone formation. BMSC cells were cultured in osteogenic media as describe above with either fresh PF-46 or P1000:G10 hydrogel-released PF-46 (0.5 μM final concentration). Cells were left unstained or stained for Ca^{2+} deposits with Alizarin S red. As shown in Figure 10B, cells cultured with either fresh PF-46 or hydrogel-eluted PF-46 showed enhanced Ca^{2+} nodule formation, indicating increased osteoblastic differentiation and mineralization.

4. Discussion

To identify an appropriate Pyk2 inhibitor, we examined the efficacy of two commercially-available small molecule inhibitors of Pyk2, namely PF-43 and PF-46. We found that PF-46, a Pyk2-targeted inhibitor, promoted osteoblast activity and mineralizing activity to a greater extent than PF-43. Our results are consistent with published studies showing that PF-46 enhanced the mineralization of osteoblasts, whereas PF-43 failed to promote mineral deposition. One possible reason for this may be that PF-43 has an IC_{50} value that is 20-fold more potent against FAK than Pyk2, suggesting it inhibits FAK more than Pyk2 [21], although this was not tested in our study. Consistent with this, it has also been reported that inhibition of FAK significantly reduces calcium deposition in human MSCs after 28 days of culture [46]. For the current studies, we focused our investigations to the use of the Pyk2-targeted inhibitor, PF-46, because of it enhanced overall osteogenic activity, including ALP and mineralization. Further, we found that PF-46 eluted from the PEDGA hydrogels retained its inhibitor activity against Pyk2, and that inhibition of Pyk2 by PF-46 enhanced both ALP activity and mineral deposition by BMSC.

In the current study, we investigated two Pyk2 inhibitor-containing hydrogels and evaluated the viscosity, gelation time, swelling, degradation, and release behavior of these hydrogels. Several of our experiments suggested that a hydrogel composed of PEGDA1000 plus 10% gelatin (P1000:G10) may make an appropriate carrier for the delivery of the Pyk2 inhibitors to promote osteoblast bone formation. We found that the P1000:G10 hydrogel was cytocompatible and that PF-46 released from the hydrogel retained its inhibitory activity against Pyk2, leading to an increase in osteoblast activity. We also found that the P1000:G10 solution exhibited the most obvious shear-thinning behavior. In addition, the P1000:G10 solution exhibited the highest viscosity when it reached the Newtonion fluid behavior. These characteristics of the P1000:G10 hydrogel make it suitable as a drug delivery carrier because its viscosity is reduced when stress is applied, and viscosity is rapidly recovered upon removal of the stress; after which it can release its drug [47] In addition, P1000:G10 solution is a yield stress fluid, which indicates that the solution will remain stationary after injection, allowing it to be cured without the concern of a free flowing solution. Thus, the viscosity and shear-thinning behavior of the P1000:G10 hydrogel may make it suitable for use as an injectable-carrier to minimize undesirable leakage into neighboring tissues or the blood circulation.

The P1000:G10 hydrogel also showed a significantly lower swelling ratio than P600:G5. This effect was possibly due to the higher amount of gelatin, which is consistent with published studies showing that when the gelatin concentration exceeds 6%, the swelling degree decreases because of a significant increase in the network chains density. This can lead to decreases in water absorption and polymer relaxation, resulting in a decrease in the degree of hydrogel swelling [48]. Our PEGDA-gelatin hydrogels consist of PEGDA chains with DTT to form $(-PEG-DTT-)_n$ PEG polymer chains, which are hydrolytically labile chains. Thus, the formed hydrogels can undergo hydrolytic degradation over time [49,

50]. In addition, we used gelatin, which is a natural polymer that is responsive to enzymatic degradation and can be degraded *in vivo* by several enzymes, such as collagenase and lysozyme [51, 52]. This suggests that our PEGDA-gelatin hydrogels can be tailored for desirable degradation time through the adjustment of the concentration of DTT and gelatin.

Although we used the same gelatin and PEGDA polymers for the synthesis of both PEGDA-gelatin hydrogels, we found that P600:G5 exhibited inferior loading efficiency compared to P1000:G10. This suggests that molecular weight of PEGDA and gelatin concentration may affect loading efficiency. It is known that the swelling and degradation of hydrogels in drug-delivery applications facilitates local delivery through temporally-modulated drug release. The release profile of AMC from both of the PEGDA-gelatin hydrogels showed an initial burst release. However, the amount of release from PEGDA-gelatin hydrogels was lower than in collagen sponges, which was likely due to P1000:G10 having a lowest degree of swelling and degradation. One limitation of this approach is that the release profile of AMC may differ from that of PF-46 due to differences in molecular weight, structure, and solubility between the two molecules. However, we also investigated the release behavior of PF-46 loaded into P1000:G10, which showed that similar to AMC, PF-46 exhibited an initial rapid release phase, followed by a slower release phase, with 100% PF-46 release being achieved by 3-4 days. Together, these data suggest that AMC can be used as a model system for initial characterization of the release profiles of hydrogel-based scaffolds, and that PEGDA-gelatin hydrogels may have broad applicability as carriers for a range of small molecules. Moreover, the % cumulative release profile of PF-46, suggests the P1000:G10 hydrogel may be useful for as a carrier for the delivery of PF-46 over several days.

To the best of our knowledge, this is the first study to develop a PEGDA-gelatin hydrogel for osteogenic applications. Notably, the Pyk2-inihbitor, PF-46, released from P1000:G10 retained its inhibitory activity against the Pyk2 tyrosine kinase and promoted ALP activity and Ca^{2+} mineral deposition by osteoblasts *in vitro*. Overall, our results indicate that P1000:G10 is an appropriate carrier for PF-46 based on several characteristics: 1) P1000:G10 prepolymer solutions exhibit a shear-thinning effect, 2) P1000:G10 prepolymer solutions exhibit Bingham fluid or yield point fluid behavior which can prevent undesirable leakage of the solution into neighboring tissues or blood circulation before polymerization, 3) P1000:G10 can form gel *in situ* by photopolymerization with a reasonable gelation time; allowing for sufficient handling time prior to light curing, 4) The P1000:G10 hydrogel is biodegradable, 5) P1000:G10 is cytocompatible and exhibited the slowest drug-release behavior compared to other hydrogel formulations we tested. Furthermore, one advantage of a hydrogel-based carrier is that the carrier and/or scaffold design can be tailored for timed drug release and degradation. All of these findings strongly support the use of PEGDA-gelatin hydrogel incorporated with a Pyk2-targeted inhibitor for targeted bone regeneration applications. Given our published reports that osteoclasts from Pyk2-deficient mice have decreased bone

resorbing activities, the Pyk2-inhibitor based hydrogels may also be useful for the treatment of localized bone loss, for example in the treatment of periodontal disease.

Acknowledgements

Grant sponsors: National Institutes of Health, NIAMS R01-AR060332; Indiana Clinical and Translational Science Institute, Collaboration in Biomedical/Translational Research (CBR/CTR) Pilot Program Grants, RR025761, TR000006; IUPUI Office of the Vice Chancellor for Research (OVCR) Research Support Funds Grant (RSFG); IUPUI Biomechanics and Biomaterials Research Center (BBRC) Grant and funds from Indiana University School of Dentistry. The authors would like to thank Dr. Marco Bottino, Indiana University School of Dentistry, for helpful suggestions and discussions. In addition, we thank Dr. Chien-Chi Lin and Tanja Greene, IUPUI School of Engineering and Technology, for guidance and assistance with the rheometry experiments.

References

[1] Amini AR, Laurencin CT, Nukavarapu SP. Bone tissue engineering: recent advances and challenges. Critical reviews in biomedical engineering. 2012;40:363-408.

[2] Oryan A, Alidadi S, Moshiri A, Maffulli N. Bone regenerative medicine: classic options, novel strategies, and future directions. Journal of orthopaedic surgery and research. 2014;9:18.

[3] Romagnoli C, D'Asta F, Brandi ML. Drug delivery using composite scaffolds in the context of bone tissue engineering. Clinical cases in mineral and bone metabolism : the official journal of the Italian Society of Osteoporosis, Mineral Metabolism, and Skeletal Diseases. 2013;10:155-61.

[4] Mourino V, Boccaccini AR. Bone tissue engineering therapeutics: controlled drug delivery in three-dimensional scaffolds. Journal of the Royal Society, Interface / the Royal Society. 2010;7:209-27.

[5] Chu TM, Warden SJ, Turner CH, Stewart RL. Segmental bone regeneration using a load-bearing biodegradable carrier of bone morphogenetic protein-2. Biomaterials. 2007;28:459-67.

[6] Mont MA, Ragland PS, Biggins B, Friedlaender G, Patel T, Cook S, et al. Use of bone morphogenetic proteins for musculoskeletal applications. An overview. J Bone Joint Surg Am. 2004;86-A Suppl 2:41-55.

[7] de Oliveira GS, Miziara MN, Silva ER, Ferreira EL, Biulchi AP, Alves JB. Enhanced bone formation during healing process of tooth sockets filled with demineralized human dentine matrix. Aust Dent J. 2013;58:326-32.

[8] Fu R, Selph S, McDonagh M, Peterson K, Tiwari A, Chou R, et al. Effectiveness and harms of recombinant human bone morphogenetic protein-2 in spine fusion: a systematic review and meta-analysis. Annals of internal medicine. 2013;158:890-902.

[9] Rodgers MA, Brown JV, Heirs MK, Higgins JP, Mannion RJ, Simmonds MC, et al. Reporting of industry funded study outcome data: comparison of confidential and published data on the safety and effectiveness of rhBMP-2 for spinal fusion. BMJ (Clinical research ed). 2013;346:f3981.

[10] Mesfin A, Buchowski JM, Zebala LP, Bakhsh WR, Aronson AB, Fogelson JL, et al. High-dose rhBMP-2 for adults: major and minor complications: a study of 502 spine cases. J Bone Joint Surg Am. 2013;95:1546-53.

[11] Simmonds MC, Brown JV, Heirs MK, Higgins JP, Mannion RJ, Rodgers MA, et al. Safety and effectiveness of recombinant human bone morphogenetic protein-2 for spinal fusion: a meta-analysis of individual-participant data. Annals of internal medicine. 2013;158:877-89.

[12] Freitas F, Jeschke M, Majstorovic I, Mueller DR, Schindler P, Voshol H, et al. Fluoroaluminate stimulates phosphorylation of p130 Cas and Fak and increases attachment and spreading of preosteoblastic MC3T3-E1 cells. Bone. 2002;30:99-108.

[13] Boutahar N, Guignandon A, Vico L, Lafage-Proust MH. Mechanical strain on osteoblasts activates autophosphorylation of focal adhesion kinase and proline-rich tyrosine kinase 2 tyrosine sites involved in ERK activation. Journal of Biological Chemistry. 2004;279:30588-99.
[14] Meyers VE, Zayzafoon M, Gonda SR, Gathings WE, McDonald JM. Modeled microgravity disrupts collagen I/integrin signaling during osteoblastic differentiation of human mesenchymal stem cells. JCell Biochem. 2004;93:697-707.
[15] Guignandon A, Boutahar N, Rattner A, Vico L, Lafage-Proust MH. Cyclic strain promotes shuttling of PYK2/Hic-5 complex from focal contacts in osteoblast-like cells. BiochemBiophysResCommun. 2006.
[16] Buckbinder L, Crawford DT, Qi H, Ke HZ, Olson LM, Long KR, et al. Proline-rich tyrosine kinase 2 regulates osteoprogenitor cells and bone formation, and offers an anabolic treatment approach for osteoporosis. Proceedings of the National Academy of Sciences of the United States of America. 2007;104:10619-24.
[17] Kacena MA, Eleniste PP, Cheng YH, Huang S, Shivanna M, Meijome TE, et al. Megakaryocytes regulate expression of Pyk2 isoforms and caspase-mediated cleavage of actin in osteoblasts. The Journal of biological chemistry. 2012;287:17257-68.
[18] Cheng YH, Hooker RA, Nguyen K, Gerard-O'Riley R, Waning DL, Chitteti BR, et al. Pyk2 regulates megakaryocyte-induced increases in osteoblast number and bone formation. Journal of bone and mineral research : the official journal of the American Society for Bone and Mineral Research. 2013;28:1434-45.
[19] Gil-Henn H, Destaing O, Sims NA, Aoki K, Alles N, Neff L, et al. Defective microtubule-dependent podosome organization in osteoclasts leads to increased bone density in Pyk2(-/-) mice. The Journal of cell biology. 2007;178:1053-64.
[20] Posritong S, Hong JM, Eleniste PP, McIntyre PW, Wu JL, Himes ER, et al. Pyk2 deficiency potentiates osteoblast differentiation and mineralizing activity in response to estrogen or raloxifene. Molecular and cellular endocrinology. 2018.
[21] Han S, Mistry A, Chang JS, Cunningham D, Griffor M, Bonnette PC, et al. Structural characterization of proline-rich tyrosine kinase 2 (PYK2) reveals a unique (DFG-out) conformation and enables inhibitor design. The Journal of biological chemistry. 2009;284:13193-201.
[22] Ratko TA, Belinson SE, Samson DJ, Bonnell C, Ziegler KM, Aronson N. Bone Morphogenetic Protein: The State of the Evidence of On-Label and Off-Label Use. Rockville MD2010.
[23] Lin CC, Anseth KS. PEG hydrogels for the controlled release of biomolecules in regenerative medicine. Pharmaceutical research. 2009;26:631-43.
[24] Lin CC, Ki CS, Shih H. Thiol-norbornene photo-click hydrogels for tissue engineering applications. J Appl Polym Sci. 2015;132.

[25] Hao Y, Lin CC. Degradable thiol-acrylate hydrogels as tunable matrices for three-dimensional hepatic culture. Journal of biomedical materials research Part A. 2014;102:3813-27.
[26] Fu Y, Kao WJ. Drug release kinetics and transport mechanisms from semi-interpenetrating networks of gelatin and poly(ethylene glycol) diacrylate. Pharmaceutical research. 2009;26:2115-24.
[27] Santoro M, Tatara AM, Mikos AG. Gelatin carriers for drug and cell delivery in tissue engineering. Journal of controlled release : official journal of the Controlled Release Society. 2014;190:210-8.
[28] Fu Y, Xu K, Zheng X, Giacomin AJ, Mix AW, Kao WJ. 3D cell entrapment in crosslinked thiolated gelatin-poly(ethylene glycol) diacrylate hydrogels. Biomaterials. 2012;33:48-58.
[29] Bruzzaniti A, Neff L, Sandoval A, Du L, Horne WC, Baron R. Dynamin reduces Pyk2 Y402 phosphorylation and SRC binding in osteoclasts. Molecular and cellular biology. 2009;29:3644-56.
[30] Gregory CA, Gunn WG, Peister A, Prockop DJ. An Alizarin red-based assay of mineralization by adherent cells in culture: comparison with cetylpyridinium chloride extraction. Analytical biochemistry. 2004;329:77-84.
[31] Emmakah AM, Arman HE, Bragg JC, Greene T, Alvarez MB, Childress PJ, et al. A fast-degrading thiol-acrylate based hydrogel for cranial regeneration. Biomedical materials (Bristol, England). 2017;12:025011.
[32] Metz J, Gonnerman K, Chu A, Chu TM. Effect of crosslinking density on swelling and mechanical properties of PEGDA400/PCLTMA900 hydrogels. Biomed Sci Instrum. 2006;42:389-94.
[33] Lin CC, Raza A, Shih H. PEG hydrogels formed by thiol-ene photo-click chemistry and their effect on the formation and recovery of insulin-secreting cell spheroids. Biomaterials. 2011;32:9685-95.
[34] Lemon JC, Okay DJ, Powers JM, Martin JW, Chambers MS. Facial moulage: the effect of a retarder on compressive strength and working and setting times of irreversible hydrocolloid impression material. J Prosthet Dent. 2003;90:276-81.
[35] Murata H, Kawamura M, Hamada T, Chimori H, Nikawa H. Physical properties and compatibility with dental stones of current alginate impression materials. J Oral Rehabil. 2004;31:1115-22.
[36] Liu WC, Ballenger B, Algarni A, Velez M, TM GC. FTIR characterization and release of bovine serum albumin from bioactive glasses. Journal of applied biomaterials & functional materials. 2017;15:e347-e55.
[37] ISO-10993-5. Biological evaluation of medical devices. Part 5: tests for cytotoxicity: in vitro methods. In: ISO, editor.1993.
[38] Glowacki J, Mizuno S. Collagen scaffolds for tissue engineering. Biopolymers. 2008;89:338-44.
[39] Golub EE, Harrison G, Taylor AG, Camper S, Shapiro IM. The role of alkaline phosphatase in cartilage mineralization. Bone and mineral. 1992;17:273-8.
[40] Moller P, Fall A, Chikkadi V, Derks D, Bonn D. An attempt to categorize yield stress fluid behaviour. Philosophical transactions Series A, Mathematical, physical, and engineering sciences. 2009;367:5139-55.

[41] Asghar W, Islam M, Wadajkar AS, Wan Y, Ilyas A, Nguyen KT, et al. PLGA Micro-and Nanoparticles Loaded Into Gelatin Scaffold for Controlled Drug Release
IEEE Transactions on Nanotectology. 2012;11:546-53.
[42] Chattopadhyay S, Raines RT. Review collagen-based biomaterials for wound healing. Biopolymers. 2014;101:821-33.
[43] Eley JG, Tirumalasetty PP. Release characteristics of polymethacrylate nanospheres containing coumarin-6. Journal of microencapsulation. 2003;20:653-9.
[44] Dash S, Murthy PN, Nath L, Chowdhury P. Kinetic modeling on drug release from controlled drug delivery systems. Acta poloniae pharmaceutica. 2010;67:217-23.
[45] Grassi M, Grassi G. Mathematical modelling and controlled drug delivery: matrix systems. Current drug delivery. 2005;2:97-116.
[46] Salasznyk RM, Klees RF, Williams WA, Boskey A, Plopper GE. Focal adhesion kinase signaling pathways regulate the osteogenic differentiation of human mesenchymal stem cells. Experimental cell research. 2007;313:22-37.
[47] Choi B, Loh XJ, Tan A, Loh CK, Ye E, Joo MK, et al. Introduction to In Situ Forming Hydrogels for Biomedical Applications. In: Loh JX, editor. In-Situ Gelling Polymers: For Biomedical Applications. Singapore: Springer Singapore; 2015. p. 5-35.
[48] Liu, Ballada A. Engineering of Polymers and Chemical Complexity, Volume I: Current State of the Art and Perspectives. New Jersy, USA: Apple Academic Press 2014.
[49] Parlato M, Reichert S, Barney N, Murphy WL. Poly(ethylene glycol) hydrogels with adaptable mechanical and degradation properties for use in biomedical applications. Macromol Biosci. 2014;14:687-98.
[50] Hudalla GA, Eng TS, Murphy WL. An approach to modulate degradation and mesenchymal stem cell behavior in poly(ethylene glycol) networks. Biomacromolecules. 2008;9:842-9.
[51] Bae JW, Choi JH, Lee Y, Park KD. Horseradish peroxidase-catalysed in situ-forming hydrogels for tissue-engineering applications. Journal of tissue engineering and regenerative medicine. 2015;9:1225-32.
[52] Hutson CB, Nichol JW, Aubin H, Bae H, Yamanlar S, Al-Haque S, et al. Synthesis and characterization of tunable poly(ethylene glycol): gelatin methacrylate composite hydrogels. Tissue engineering Part A. 2011;17:1713-23.

FIGURE 1. The efficacy of PF-43 and PF-46 on osteoblast activity. A) Bone marrow stromal osteoblasts were treated with a dual FAK/Pyk2 inhibitor (PF-43) or a Pyk2-targeted inhibitor (PF-46) at 0.1 and 0.3 μM for 24 hours. Proliferation activity was determined using an MTS assay. B and C) Bone marrow stromal osteoblasts were differentiated into mature osteoblasts under osteogenic conditions for 7 or 21 days in the presence or absence of PF-43 or PF-46, and the ALP activity and mineralization assays were performed, respectively. Control indicates DMSO vehicle, which was used to solubilize the inhibitors. The data are shown as mean and SEM of triplicate samples. Experiments were performed a minimum of three times and representative data are shown. Asterisks (*) indicate statistical significance ($p<0.05$).

FIGURE 2: Schematic representation of the preparation of hydrogels and subsequent characterization and cell-based studies. See methods for details.

FIGURE 3. The dynamic viscosity of PEGDA and PEGDA-gelatin hydrogels. The dynamic viscosity of P600, P600:G5, P1000, and P1000:G10 prepolymer solutions was measured using a digital rheometer (viscometry mode) at room temperature was performed. The plots of A) viscosity versus shear rate, and B) shear stress versus shear rate of a representative sample from each group are shown.

FIGURE 4. The gelation times of PEGDA and PEGDA-gelatin hydrogels. P600, P600:G5, P1000, and P1000:G10 prepolymer solutions were prepared and pipetted into the disk-shaped mold of 5 mm in diameter and 3 mm in thickness and exposed under visible light at room temperature. Gelation times were determined using a periodontal probe to verify the hardened of materials' surfaces. The data are shown as mean and SEM of five samples (N=5). Asterisks (*) indicate statistical significant differences between different molecular weights of PEGDA, while the pound sign (#) shows the significant effect of gelatin ($p<0.05$).

FIGURE 5. The swelling ratio and degradation of PEGDA-gelatin hydrogels. A) P600:G5 and P1000:G10 gels were prepared and dried under the vacuum for 48 hours before soaking gels in PBS at 37°C and weight measuring up to 25 days. The swelling ratios for the first four hours are shown in the insert. B) The degradation of P600:G5 and P1000:G10 gels were also evaluated using the same method as the swelling experiment. The data are shown as mean and SEM of five samples (N=5). Experiments were performed twice and representative data are shown. Asterisks (*) indicate statistical significance ($p<0.05$).

FIGURE 6. FTIR analysis of PEGDA 600 (P600), 10% gelatin stock solution, cured P600:G5, PEGDA 1000 (P1000), 20% gelatin stock solution, and cured P1000:G10 are shown. Samples were prepared in triplicate for each solution, and a representative FTIR readout is shown.

FIGURE 7. The release profiles of PEGDA-gelatin hydrogels. To estimate drug elution, we used the 7-amino-4-methylcoumarin dye. The dye was loaded into P600:G5 and P1000:G10 hydrogels or the collagen sponge (control) (N=5). The carriers were incubated in PBS at 37 °C, and aliquots of PBS were collected up to 25 days. A) The cumulative amount of dye released from carriers was determined by spectrophotometry. B) The plots of % cumulative release vs. time square root of the three candidate carriers are shown for the whole period of release. The insert shows the plot of the first 60% cumulative release versus time square root of all carriers. The correlation efficient (R^2) and slope (y) for each candidate are also indicated. C) The PEGDA1000 plus 10% gelatin hydrogel was loaded with PF-46 and then cured. Aliquots of PF-46 in αMEM were taken at 1-96 hours as indicated, with replacement of equal volume of media. PF-46 elution was determined on a spectrophotometer (after subtraction of a DMSO baseline) and quantified using a standard curve generated by serial dilution of fresh PF-46. The % cumulative release of PF-46 is shown. Each point is mean of triplicate samples with error bars representing SEM.

FIGURE 8. *In vitro* cytotoxicity of PEGDA-gelatin containing eluates. P600:G5 and P1000:G10 hydrogels, and collagen sponge disks were prepared and immersed in fresh culture media at 37ºC for 24 hours, and eluates were collected. MC3T3-E1 cells were then cultured in the presence or absence of eluates for 24 hours. An MTS assay was performed to determine the proliferation/cytotoxicity of eluates. Non-

treated MC3T3-E1 cells were used as a positive control. The data are shown as mean and SEM of N=5. Experiments were performed twice and representative data are shown.

FIGURE 9. Inhibition of Pyk2 tyrosine kinase activity by hydrogel-released PF-46. PF-46 loaded P1000:G10 gels were immersed in culture media at 37ºC for 24 hours. Released PF-46 in each sample was collected. 293VnR cells expressing Pyk2 cDNA were cultured with PF-46 eluates or control media for 2 hours. A) Pyk2 was immunoprecipitated (IP) from cells and blotted for Pyk2 as controls. (b) The effect of released PF-46 on the intracellular Pyk2 tyrosine kinase activity was examined using the Universal Tyrosine Kinase Assay Kit. The data are shown as mean and SEM of five samples (N=5). Experiments were performed twice and representative data are shown. Asterisks (*) indicate statistically significant differences from the Pyk2 transfection control group ($p<0.05$).

FIGURE 10. Effect of released PF-46 on ALP activity in osteoblasts. The PF-46 loaded P1000:G10 gel was immersed in culture media at 37ºC for 24 hours, and released PF-46 was collected. Bone marrow derived stromal osteoblasts were differentiated into mature osteoblasts under osteogenic conditions in the presence or absence of released PF-46 at various concentrations, which was estimated based on the PF-46 and AMC elution profiles (Figure 7). A) ALP activity was assayed after 7 days. PF-46 that was freshly prepared or incubated for 24-hour at 37ºC prior to cell culture were used as positive controls. Vehicle treated cells (0) were used as the negative control. Asterisks (*) indicate statistically significant differences from the negative control ($p<0.05$). Significance between fresh and released PF-46 are also indicated (#). The data are shown as mean and SEM of five samples (N=5). Experiments were performed twice and representative data are shown. B) Osteoblasts were cultured in osteogenic media containing either fresh PF-46 (0.5 μM) or PF-46 eluted from P1000:G10 (estimated concentration of 0.5 μM), or an equivalent volume of the DMSO vehicle control. Representative bright field microscopic images are shown. Scale bar indicates 50 microns. Osteoblasts were also stained with Alizarin S red to stain Ca^{2+} mineral deposits, and imaged. Representative images are shown.

Figure 1

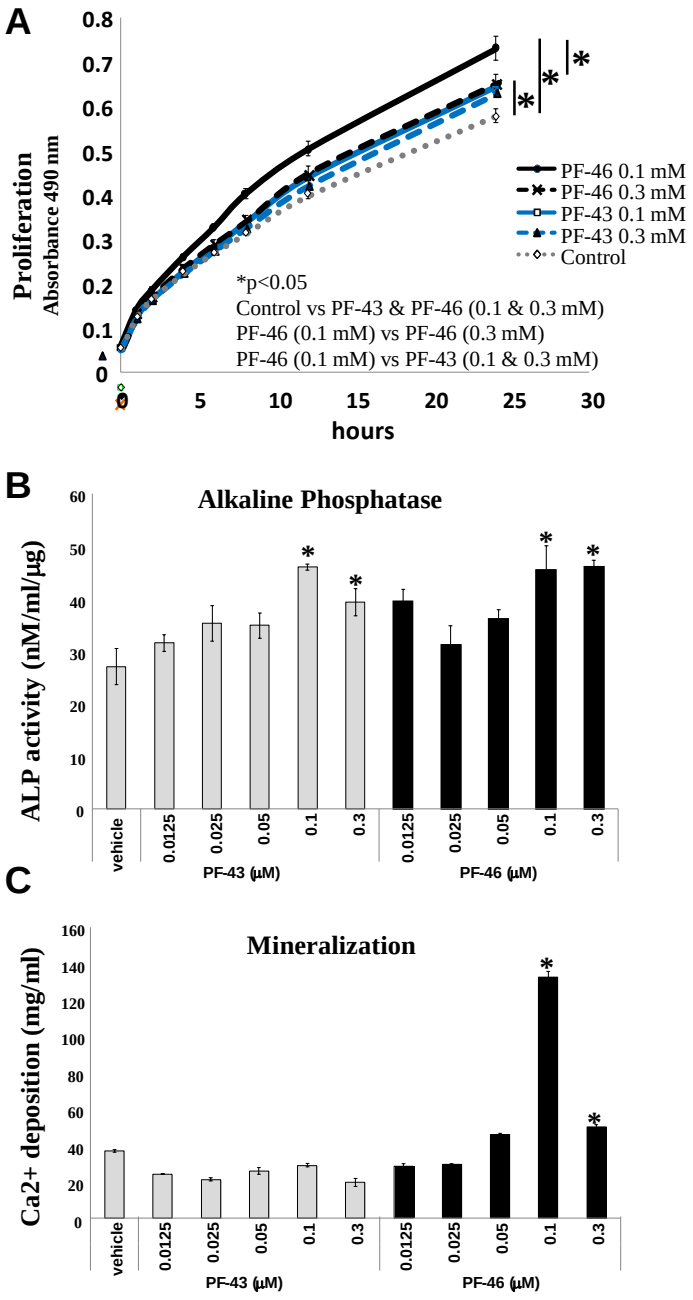
A
Proliferation
Absorbance 490 nm
0.8
0.7
0.6
0.5
0.4
0.3
0.2
0.1
0
0
5
10
15
20
25
30
hours
PF-46 0.1 mM
PF-46 0.3 mM
PF-43 0.1 mM
PF-43 0.3 mM
Control
*p<0.05
Control vs PF-43 & PF-46 (0.1 & 0.3 mM)
PF-46 (0.1 mM) vs PF-46 (0.3 mM)
PF-46 (0.1 mM) vs PF-43 (0.1 & 0.3 mM)
B
Alkaline Phosphatase
ALP activity (nM/ml/µg)
60
50
40
30
20
10
0
vehicle
0.0125
0.025
0.05
0.1
0.3
PF-43 (µM)
0.0125
0.025
0.05
0.1
0.3
PF-46 (µM)
C
Mineralization
Ca2+ deposition (mg/ml)
160
140
120
100
80
60
40
20
0
vehicle
0.0125
0.025
0.05
0.1
0.3
PF-43 (µM)
0.0125
0.025
0.05
0.1
0.3
PF-46 (µM)

Figure 2

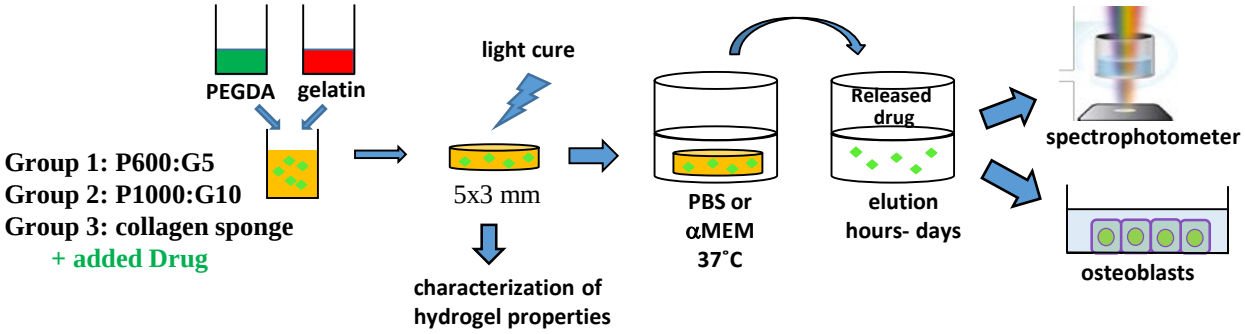
PEGDA
gelatin
Group 1: P600:G5
Group 2: P1000:G10
Group 3: collagen sponge
+ added Drug
light cure
5x3 mm
characterization of
hydrogel properties
PBS or
αMEM
37˚C
Released
drug
elution
hours- days
spectrophotometer
osteoblasts

Figure 3

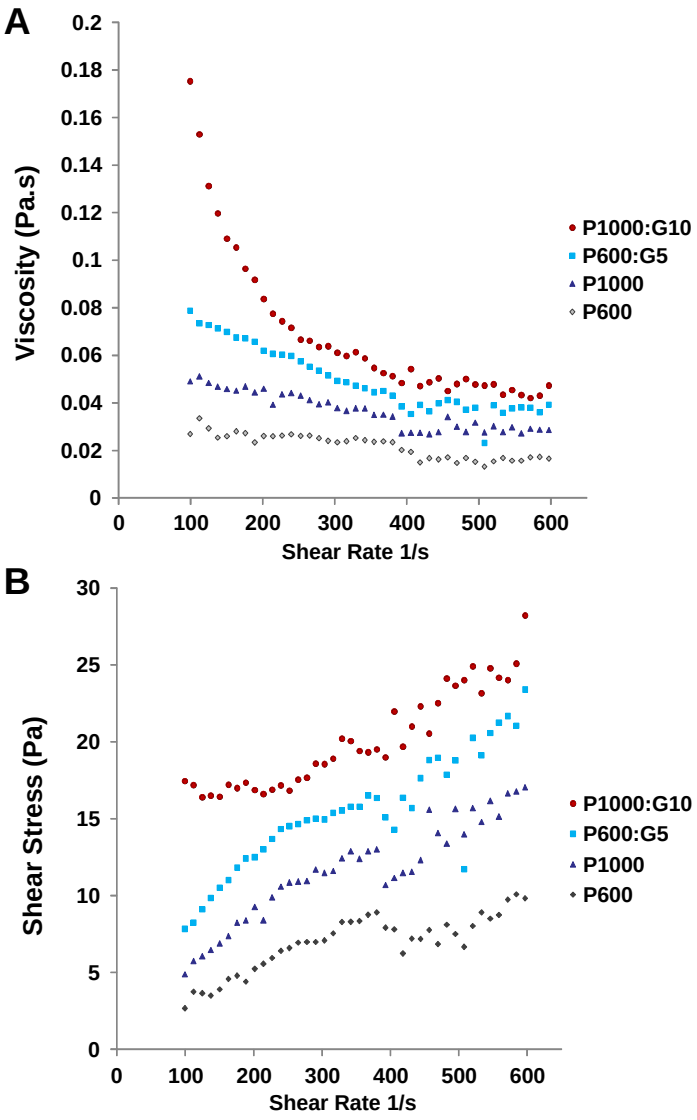
A
Viscosity (Pa.s)
0.2
0.18
0.16
0.14
0.12
0.1
0.08
0.06
0.04
0.02
0
0
100
200
300
400
500
600
Shear Rate 1/s
P1000:G10
P600:G5
P1000
P600
B
Shear Stress (Pa)
30
25
20
15
10
5
0
0
100
200
300
400
500
600
Shear Rate 1/s
P1000:G10
P600:G5
P1000
P600

Figure 4

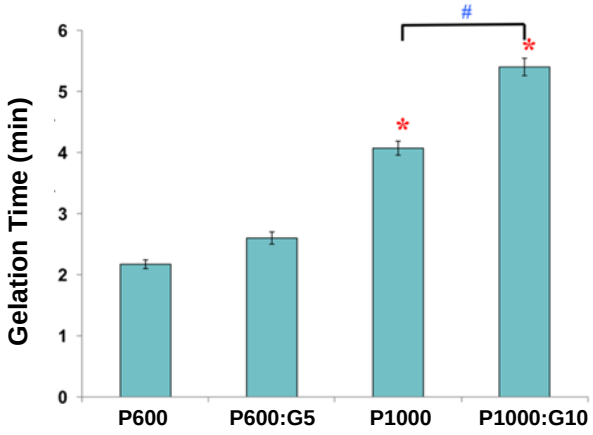

Figure 5

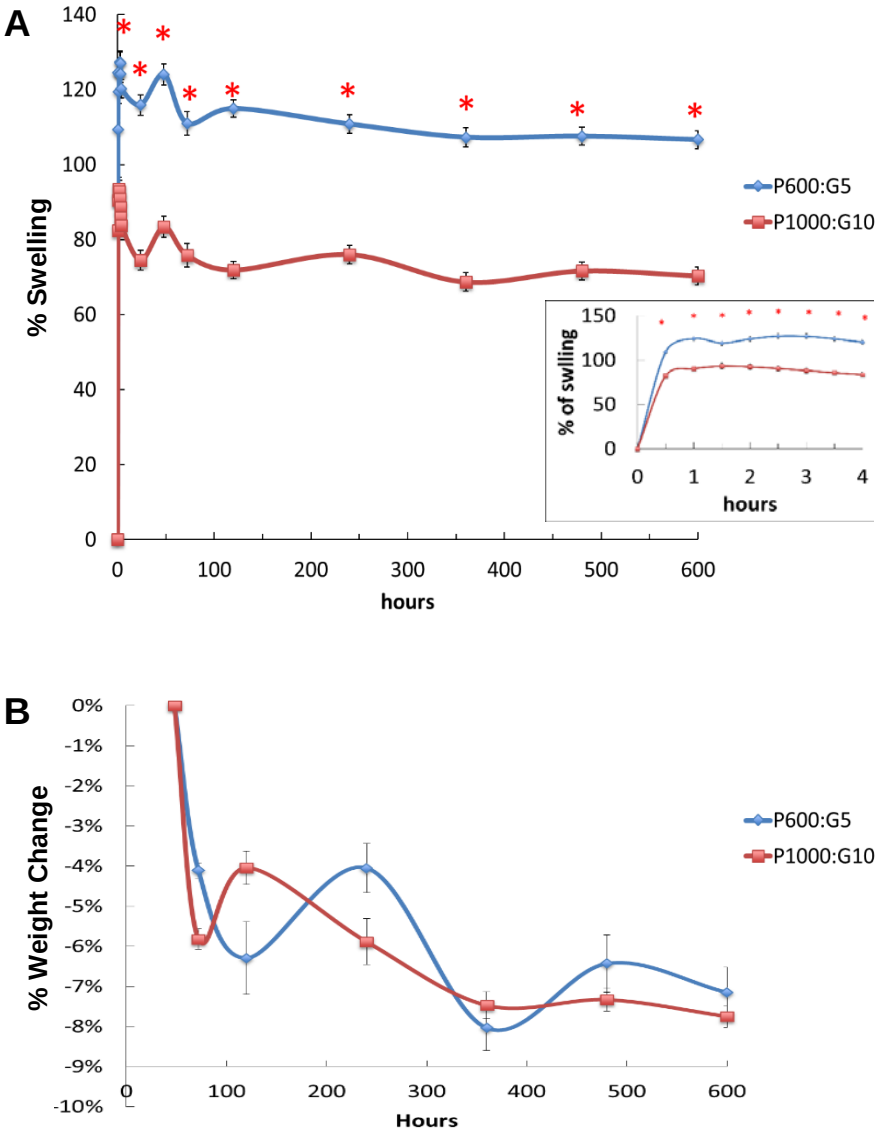
A
% Swelling
hours
P600:G5
P1000:G10
% of swlling
hours
B
% Weight Change
Hours
P600:G5
P1000:G10

Figure 6

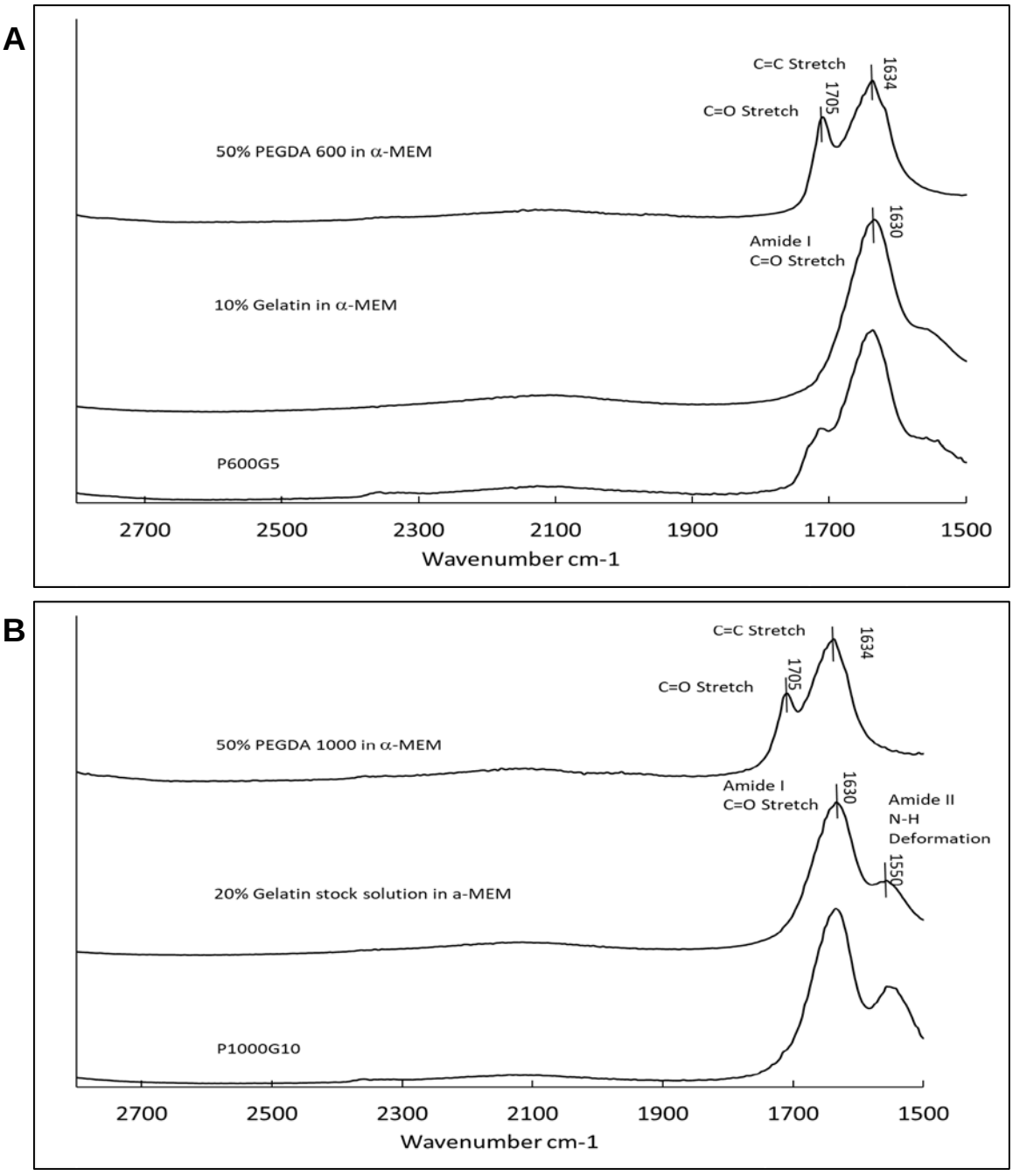
A
C=C Stretch
1634
C=O Stretch
1705
50% PEGDA 600 in α-MEM
1630
Amide I
C=O Stretch
10% Gelatin in α-MEM
P600G5
2700
2500
2300
2100
1900
1700
1500
Wavenumber cm-1
B
C=C Stretch
1634
C=O Stretch
1705
50% PEGDA 1000 in α-MEM
Amide I
C=O Stretch
1630
Amide II
N-H
Deformation
1550
20% Gelatin stock solution in a-MEM
P1000G10
2700
2500
2300
2100
1900
1700
1500
Wavenumber cm-1

Figure 7

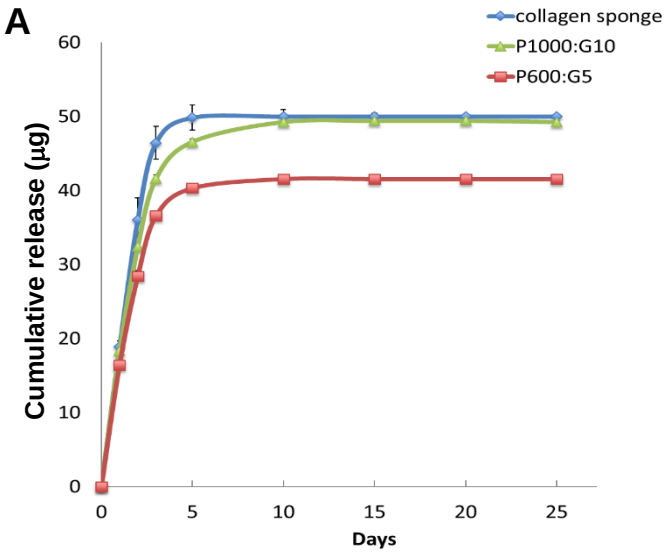
A
collagen sponge
P1000:G10
P600:G5
Cumulative release (µg)
60
50
40
30
20
10
0
0
5
10
15
20
25
Days

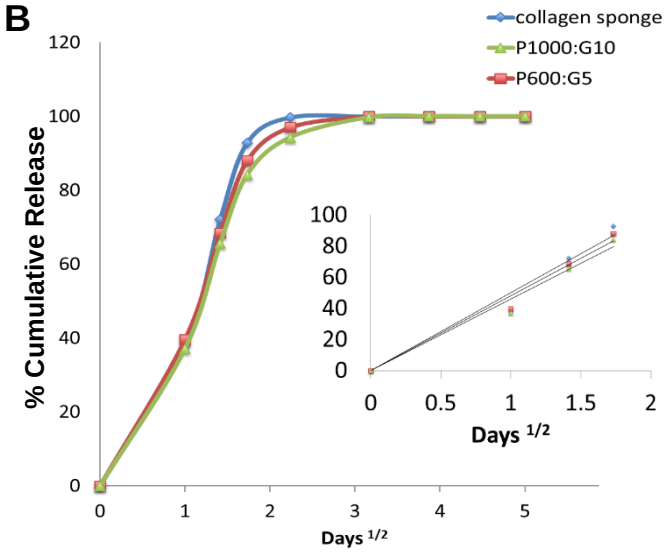
B
collagen sponge
P1000:G10
P600:G5
% Cumulative Release
120
100
80
60
40
20
0
0
1
2
3
4
5
Days 1/2
100
80
60
40
20
0
0
0.5
1
1.5
2
Days 1/2

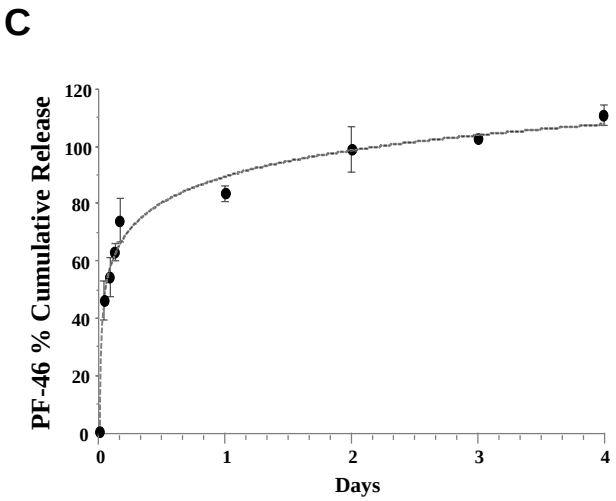
C
PF-46 % Cumulative Release
120
100
80
60
40
20
0
0
1
2
3
4
Days

Figure 8

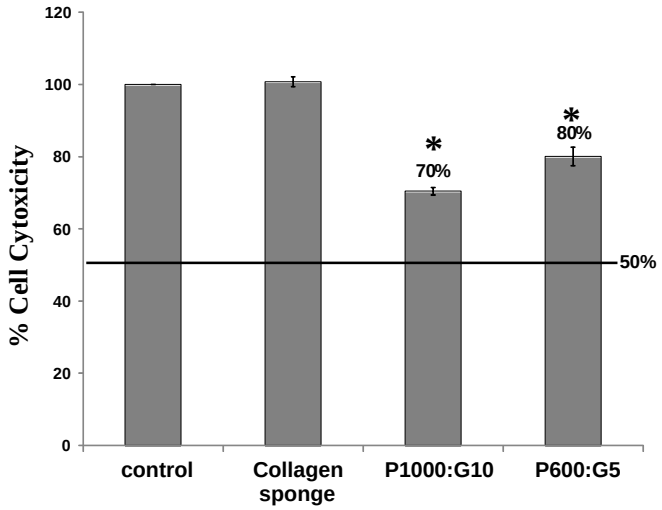
120
100
80
60
40
20
0
% Cell Cytoxicity
*
70%
*
80%
50%
control
Collagen sponge
P1000:G10
P600:G5

Figure 9

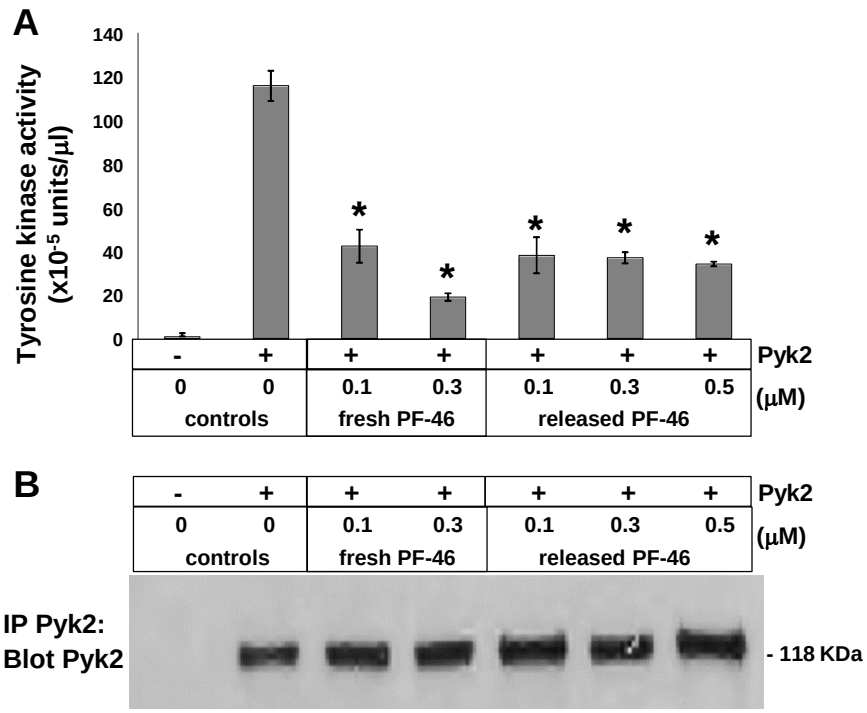
A
Tyrosine kinase activity (x10-5 units/μl)
140
120
100
80
60
40
20
0
*
*
*
*
*
-
+
+
+
+
+
+
Pyk2
0
0
0.1
0.3
0.1
0.3
0.5
(μM)
controls
fresh PF-46
released PF-46
B
-
+
+
+
+
+
+
Pyk2
0
0
0.1
0.3
0.1
0.3
0.5
(μM)
controls
fresh PF-46
released PF-46
IP Pyk2:
Blot Pyk2
- 118 KDa

Figure 10

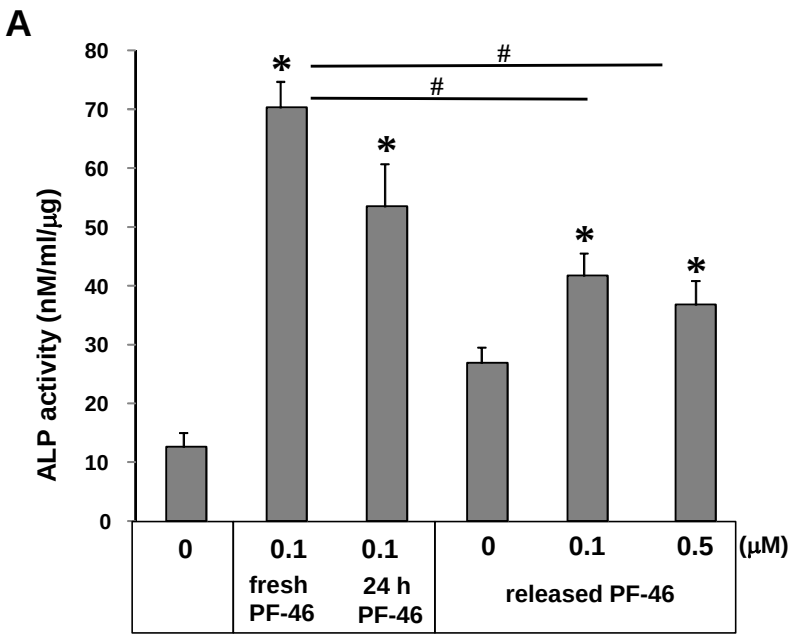
A
ALP activity (nM/ml/μg)
80
70
60
50
40
30
20
10
0
*
*
*
*
#
#
0
0.1
fresh PF-46
0.1
24 h PF-46
0
0.1
0.5
released PF-46
(μM)

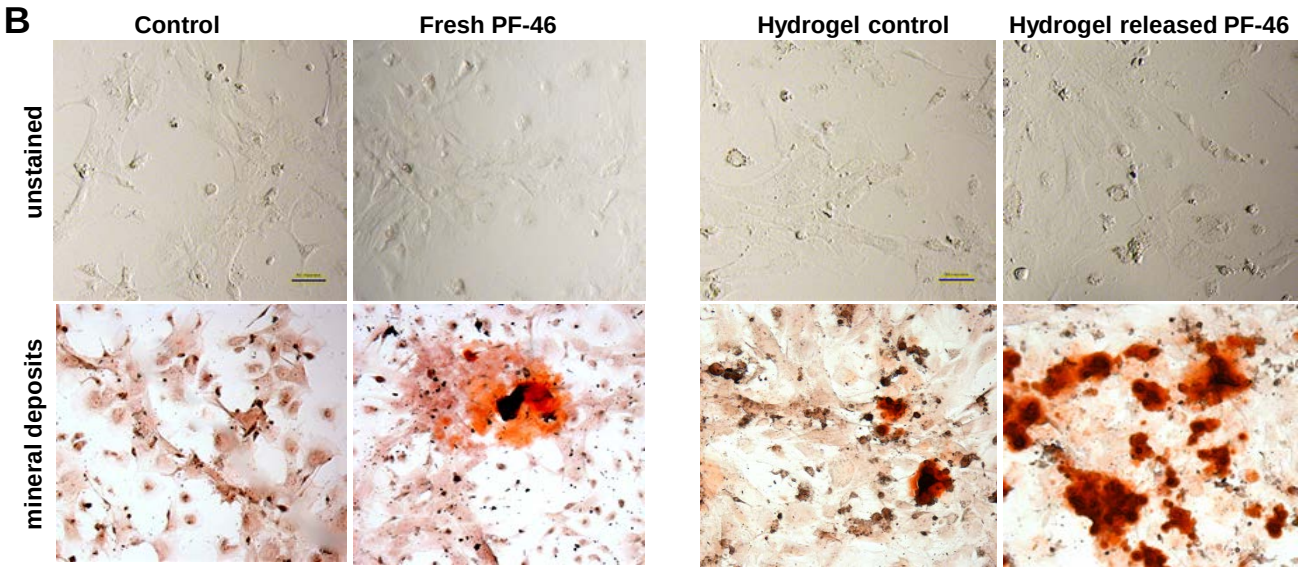
B
Control
Fresh PF-46
Hydrogel control
Hydrogel released PF-46
unstained
mineral deposits